Available online at www.sciencedirect.com

ScienceDirect

Scripta Materialia 87 (2014) 37–40

Scripta MATERIALIA

www.elsevier.com/locate/scriptamat

# Stacking fault effects on dynamic strain aging in a Ni–Co-based superalloy

Y.J. Xu,[a] D.Q. Qi,[a,c] K. Du,[a,*] C.Y. Cui[b] and H.Q. Ye[a]

[a]*Shenyang National Laboratory for Materials Science, Institute of Metal Research, Chinese Academy of Sciences, Shenyang 110016, People's Republic of China*

[b]*Superalloys Division, Institute of Metal Research, Chinese Academy of Sciences, Shenyang 110016, People's Republic of China*

[c]*School of Materials and Metallurgy, Northeast University, Shenyang 110004, People's Republic of China*

Received 25 March 2014; revised 22 May 2014; accepted 24 May 2014
Available online 12 June 2014

In this work, statistical analyses are conducted to measure the stacking fault density and stacking fault energy in a Ni–Co-based superalloy at different deformation temperatures and strain rates. High stacking fault density and low stacking fault energy indicate that the dynamic strain aging effects are caused by Suzuki segregation, which is enhanced by serious intersections of stacking faults in the superalloy. These results provide new insight into understanding stacking fault effects on dynamic strain aging in engineering alloys.



*Keywords:* Stacking fault; Dynamic strain aging; Deformation; Superalloy

Stacking fault energy (SFE) and density were measured for a Ni–Co-based superalloy at different temperatures. High stacking fault (SF) densities were observed in deformed alloys between 623 and 773 K, which are correlated to dynamic strain aging (DSA) during deformation. The highest density was determined to occur at 723 K, where an inverse DSA exists. The SFE increases with temperature, except for a sharp drop between 623 and 723 K associated with the increasing SF density.

The DSA effect, which is also known as the Portevin–Le Chatelier effect, is normally revealed by a serrated stress–strain relationship during plastic deformation [1–13]. It is generally believed that the DSA effect is caused by pinning or unpinning processes between solute atoms and mobile dislocations [1,5–9,12]. The pinning process, which corresponds to the segregation of solute atoms around dislocations, may induce an increase in the flow stress. On the contrary, the unpinning process, which corresponds to the escape of dislocations from the pinning of solute atoms, will cause a drop in the stress [12]. Research also indicates that Suzuki segregation can also play an important role in the DSA effect due to interactions between solute atoms and SF ribbons [3,4,13].

A Ni–Co-based superalloy with advanced mechanical properties at elevated temperature has been developed in recent years [14–18]. However, during plastic deformation at intermediate temperatures, two types of DSA effects have been observed in this alloy [10]. One is the normal DSA effect, which relates to an increasing critical strain leading to a serrated stress–strain relationship with rising strain rate; while the other is the inverse DSA effect, which corresponds to a decreasing critical strain with increasing strain rate. Nevertheless, the structural evolutions and influence of temperature and strain rate on the deformation behaviors are still unclear in this superalloy. In this work, we have performed statistical analyses on SF density and SFE for the superalloy deformed at different temperatures and strain rates to elucidate the influence of SFs on DSA effects in the superalloy.

The superalloy ingot was made by vacuum induction melting. It was then hot-extruded, followed by heat treatment at 1373 K for 4 h, 923 K for 24 h (air cooling) and 1033 K for 16 h (air cooling) [10,18]. Samples with dimensions of 3 mm diameter × 16 mm were made from

* Corresponding author. Tel.: +86 24 8397 0725; fax: +86 24 2389 1320; e-mail: kuidu@imr.ac.cn

http://dx.doi.org/10.1016/j.scriptamat.2014.05.012
1359-6462/

**Table 1.** Studied samples with different deformation conditions and DSA types.

| Sample | Temperature (K) | Strain rate ($s^{-1}$) | True strain (%) | DSA type |
|---|---|---|---|---|
| S298L10 | 298 | $8 \times 10^{-5}$ | 10 | N/A |
| S473L10 | 473 | $8 \times 10^{-5}$ | 10 | N/A |
| S623L10 | 623 | $8 \times 10^{-5}$ | 10 | Normal DSA [10] |
| S723L10 | 723 | $8 \times 10^{-5}$ | 10 | Inverse DSA [10] |
| S723L0.5 | 723 | $8 \times 10^{-5}$ | 0.5 | Inverse DSA [10] |
| S723L3 | 723 | $8 \times 10^{-5}$ | 3 | Inverse DSA [10] |
| S773L10 | 773 | $8 \times 10^{-5}$ | 10 | Inverse DSA [10] |
| S998L10 | 998 | $8 \times 10^{-5}$ | 10 | N/A |
| S298M10 | 298 | $3 \times 10^{-4}$ | 10 | N/A |
| S623M10 | 623 | $3 \times 10^{-4}$ | 10 | Normal DSA [10] |
| S723M10 | 723 | $3 \times 10^{-4}$ | 10 | Inverse DSA [10] |
| S773M10 | 773 | $3 \times 10^{-4}$ | 10 | Inverse DSA [10] |
| S723H10 | 723 | $3 \times 10^{-3}$ | 10 | Normal DSA [10] |

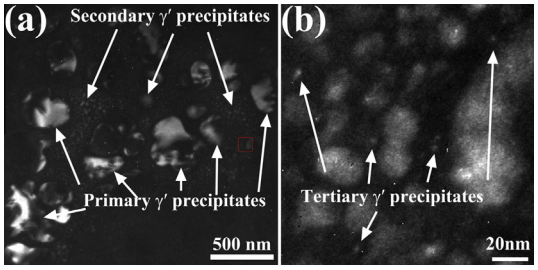


**Figure 1.** (a) Low-magnification dark-field TEM image of a typical microstructure before the deformation. (b) High-magnification image from the red box area in (a), bright contrast corresponds to $\gamma'$ phase, where tertiary $\gamma'$ precipitates are indicated by white arrows. (For interpretation of the references to colour in this figure legend, the reader is referred to the web version of this article.)

the superalloy for tensile tests. Mechanical tests were conducted on a Shimadzu 250 KN machine. Deformation temperatures and strain rates are listed in Table 1. The nominal chemical composition of the alloy was 21.8% Co, 14.4% Cr, 6.2% Ti, 2.7% Mo, 2.3% Al, 1.1% W, 0.03% Zr, 0.02% C, 0.02% B (wt.%), and balance was Ni [10]. Transmission electron microscopy (TEM) specimens were prepared from the deformed samples by conventional grinding, dimpling and ion-milling (Gatan 691 precision ion polishing system). Microstructures were investigated with a FEI Tecnai F30 electron microscope operating at 300 kV.

Figure 1 shows the microstructure of the alloy before the deformation, revealing primary, secondary and tertiary $\gamma'$ precipitates with sizes of 500–200, 100–30 and <15 nm, respectively. A high-magnification micrograph shows the tertiary $\gamma'$ precipitates in the alloy (Fig. 1b).

After tensile deformation at different temperatures and strain rates, the microstructures of the superalloy were investigated by TEM (Fig. 2). Figure 2a and d show typical low-magnification TEM and high-resolution (HR) TEM images of the sample deformed at room temperature, respectively. For the deformation at 773 K, high densities of SFs (indicated by arrows) can be seen in sample S773L10 (Fig. 2b). The HRTEM image of the sample shows intersections of SFs on non-parallel {1 1 1} planes (Fig. 2e). When the deformation temperature was increased to 998 K, twinning was observed as the dominant deformation mechanism [18]. Figure 2c shows abundant nanometer-scale deformation twins and a few SFs in the alloy. Selected-area electron diffraction clearly demonstrates the existence of twin lamellae in the specimen (inset of Fig. 2c). An

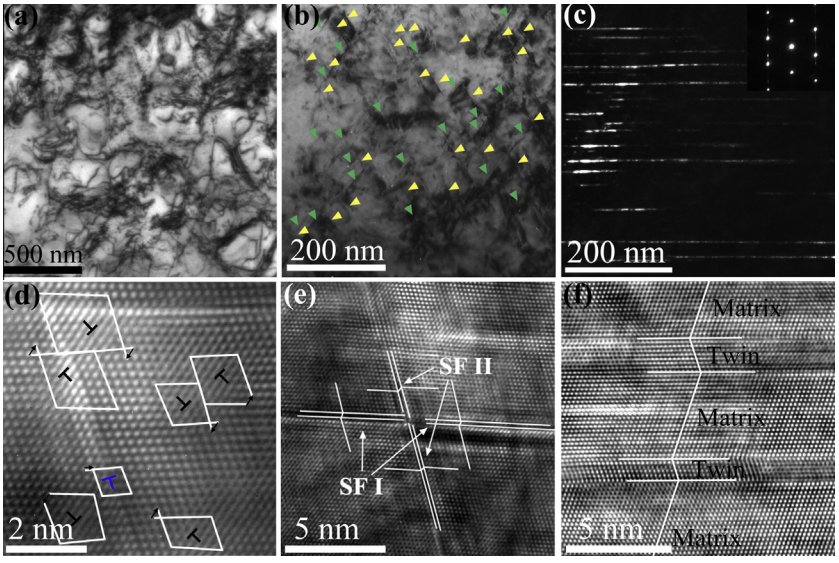


**Figure 2.** TEM (a, b, c) and HRTEM (d, e, f) images of samples deformed by tensile testing at different temperatures with a strain rate of $8 \times 10^{-5}$ $s^{-1}$: (a, d) 298 K; (b, e) 773 K; (c, f) 998 K.